Acta Cryst. (1953). **6**, 678

The Structure of Sodium Thymonucleate Fibres. II. The Cylindrically Symmetrical Patterson Function

BY ROSALIND E. FRANKLIN* AND R. G. GOSLING

Wheatstone Physics Laboratory, King's College, London W.C. 2, England

(*Received* 6 *March* 1953)

The positions and maximum photographic intensities of reflexions have been measured on X-ray microphotographs of highly crystalline sodium thymonucleate fibres. A procedure is described for deducing from these measurements the integrated intensities of the reflexions. These have been used to calculate the cylindrically symmetrical Patterson function. From this Patterson function it was possible to obtain the unit cell and hence to allot indices to all the 66 observed reflexions. Confirmation of the correctness of the indexing was obtained from photographs of a single fibre which showed double orientation of the crystallites.

Measurements of the density of wet and dry Na DNA are described, and the possible shape of the fundamental structural unit is discussed.

Introduction

In the preceding paper it was shown that by varying the water content of highly orientated fibres of sodium desoxyribonucleate (NaDNA) different structural modifications could be obtained. The most highly ordered structure was that obtained when operating at about 75% r.h. (structure *A*). This has therefore been selected for a systematic quantitative study.

The fibre diagram of this crystalline structure (Franklin & Gosling, 1953*a*, Fig. 1) shows 66 independent reflexions distributed on nine well defined layer lines. During the course of attempts to index the reflexions it became fairly clear that the unit cell was monoclinic *C*-face-centred, with the *c* axis parallel to the fibre axis. However, owing to the inevitable errors of measurement, and to the ambiguities of indexing reflexions at large angles of diffraction, it was not found possible, by direct inspection, to establish all the cell parameters with certainty. It was therefore decided to calculate the cylindrically symmetrical Patterson function described by MacGillavry & Bruins (1948). This function contains all the information which can be obtained from the fibre diagram without allotting to the reflexions any indices other than their layer-line numbers, and is therefore periodic in the *c* direction only. It is the function which would result from taking the true three-dimensional Patterson function, giving it cylindrical symmetry by rotating it about an axis through the origin and parallel to the fibre axis, and then taking a section through the axis of rotation.

The principal periodicities, or lattice translations, other than that corresponding to the layer-plane spacing, will be revealed as important peaks in this aperiodic Patterson function. They will, in general, be distinguished from other Patterson peaks in that their second (and higher) orders will be observed.

MacGillavry & Bruins (1948) have shown that the cylindrically symmetrical Patterson function $\varphi(z, x)$ is given by the equations

$$\varphi_l(x) = \frac{2\pi}{NV}\int_0^\infty H(l, \xi').J_0(2\pi\xi' x).\xi'.d\xi' \qquad (1)$$

and

$$\varphi(z, x) = \sum_l \varphi_l(x) \cos 2\pi l z\,. \qquad (2)$$

Here $\xi' = \xi/\lambda$, where ξ is the Bernal coordinate†; $H(l, \xi')$ is the intensity on the lth layer line at a distance ξ' from the fibre axis in R-space; $J_0(u)$ is the zero-order Bessel function of u; V is the volume irradiated and N is the total number of periods in the fibre direction.

If each layer-line shows only discrete reflexions whose integrated intensities can be measured, the integral in equation (1) may be replaced by a summation, and

$$\varphi_l'(x) = \sum_{\xi'} I(l, \xi').J_0(2\pi\xi' x)\,, \qquad (3)$$

where $I(l, \xi')$ is the integrated intensity of a reflexion occurring on the lth layer-line at a distance ξ' from the fibre axis, and $\varphi_l'(x) = NV\varphi_l(x)$.

Experimental

Measurements were made on photographs taken with a specimen–film distance of 15 mm. using the Philips micro-camera and an Ehrenberg–Spear fine-focus tube, as described in the preceding paper. A constant stream

* Present address: Department of Physics, Birkbeck College, London W.C. 1, England.

† MacGillavry & Bruins refer to ξ' (their ξ) as the Bernal coordinate but we have preferred to use Bernal's original notation in the discussion which follows, and so have introduced it here.

of hydrogen at 75% r.h. was passed through the camera during the exposures.

In order to search for further reflexions on or near the fibre-axis direction, photographs were also taken with the fibre inclined to the X-ray beam at a series of angles in the range 85° to 70°. A micro-camera was designed specifically for this purpose and will be described elsewhere. The specimen–film distance and collimator dimensions were the same as those of the Philips micro-camera.

These photographs revealed only one reflexion not observed with the fibre perpendicular to the X-ray beam. This reflexion lies on the 11th layer line on, or close to, the fibre-axis direction. It is, however, a weak reflexion and in the quantitative work described here its intensity, when corrected for geometrical factors, is negligibly small.

For the measurement of the R-space co-ordinates and the intensities of the 66 independent reflexions standard methods could not be applied owing to the small size of the photographs, and to the variety of shapes and sizes of the photographic spots. A description of the methods used is given below.

Measurement of R-space co-ordinates

For the measurement of the positions of reflexions the microphotographs were projected on a white cardboard screen using a magnification of about 10. The centres of the reflexions were then marked on the card and their x and y co-ordinates were measured. For the outer reflexions an indication of the length of the arcs was also recorded. The use of the projector rather than a travelling microscope was found not only to be much less fatiguing, but also to provide a more reliable estimate of the positions of weak reflexions and a more convenient method of making measurements on curved layer lines.

For calibration of the scale of the projected photographs, photographs taken with a Unicam single-crystal camera were used. In this way, the very strong equatorial reflexion was shown to correspond to a spacing of 11·3 Å. Using this value, the appropriate demagnification factor for converting the measured x and y co-ordinates to the scale of a Bernal chart was calculated, and hence the ξ and ζ values of each reflexion were obtained.

Correction for tilting of the fibre axis

A correction must be applied to the measured ξ and ζ values owing to the fact that it is almost impossible to place the fibre exactly perpendicular to the X-ray beam.

Fig. 1(*a*) illustrates the diffraction conditions when the fibre axis deviates from the ideal position by a small angle γ. A plane parallel to the layer lines and at a distance from the R-space origin, O, given by $\zeta_s = \sin\gamma$, will give a straight line l_s on the flat film. Layer planes above ζ_s will form layer lines which are less curved and have reflexions more widely separated than if the fibre were normal to the direct beam. Layer planes lying below ζ_s will form layer lines more highly curved, having reflexions closer to the meridian. The general form of the layer lines will be as indicated in Fig. 1(*b*).

Let ζ_1 and ζ_2 be the apparent ζ-values measured above and below the equator respectively for a given set of reflexions corresponding to a spacing $d = \lambda/\varrho$. It can be shown that the required value of ζ for the perpendicular fibre is given by

$$\zeta = \zeta_1 \cos\gamma + \tfrac{1}{2}\varrho^2 \sin\gamma = \zeta_2 \cos\gamma - \tfrac{1}{2}\varrho^2 \sin\gamma\,, \quad (4)$$

whence

$$\tan\gamma = (\zeta_2 - \zeta_1)/\varrho^2 \quad (5)$$

and

$$\zeta = \cos\gamma\,.(\zeta_2 + \zeta_1)/2\,. \quad (6)$$

Measurements of ζ_1, ζ_2 and ϱ can therefore be used to determine γ.

Most of our measurements were made on photographs for which γ was found to be about 8°. Values of ζ obtained with the aid of equations (4) and (5) from measurements made on reflexions in the first 9 layer

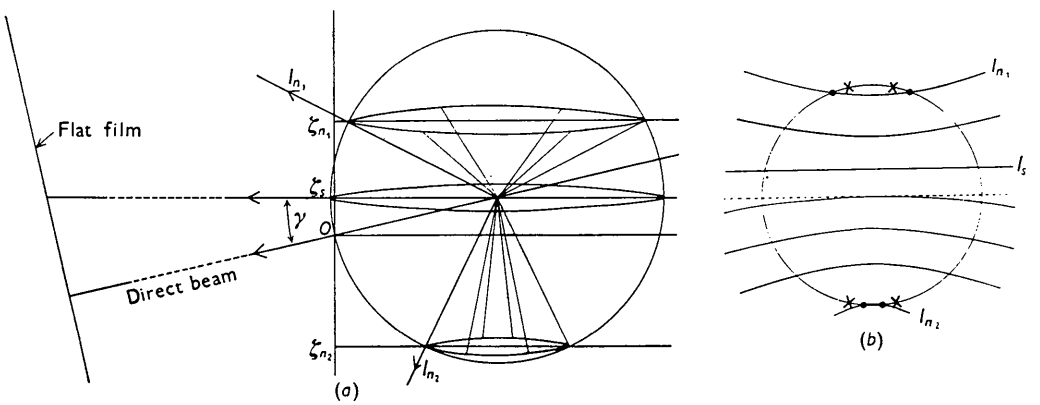

Fig. 1. (*a*) Reciprocal lattice planes and reflecting sphere for tilted fibre. (*b*) Appearance of photograph for diffraction conditions shown in (*a*). × : position of equivalent reflexions with fibre normal to X-ray beam; • : position of equivalent reflexions for fibre inclined $(90-\bar{\gamma})$ to X-ray beam.

Table 1

L	1	2	3	4	5	6	7	8	9
ζ	0·0550	0·0540	0·0533	0·0545	0·0552	0·0548	0·0545	0·0546	0·0551

lines are shown in Table 1. Each value is a mean of measurements on at least three reflexions. Neglecting the value obtained for the 3rd layer line, where the reflexions are weak and difficult to measure accurately, the mean value of ζ is 0·0547. This gives c, the fibre-axis repeat period, as 28·1 Å.

Having established in this way the layer-line spacing, values of ξ can now be obtained with improved accuracy for reflexions on the higher layer lines. For these, the most accurately observable parameter is the radius of the circle on which the four equivalent photographic spots must lie. This gives ϱ $(= \lambda/d)$, and ξ-values were therefore determined from the relationship $\xi^2 = \varrho^2 - (l\lambda/c)^2$.

Measurement of intensities

The variety of shapes and sizes of the photographic spots makes it impossible to estimate directly the integrated photographic intensity. It is necessary therefore *either* to explore each spot photometrically, *or* to estimate its maximum intensity and to consider separately the question of spot size and shape. The latter alternative was adopted. Not only would the photometric method involve a very large amount of work, but, in the micro-photographs available, the grain size is too large in relation to the spot size for photometry to be applied with any degree of accuracy. Use of fine-grain films would lead to excessive exposure times and thus remove the advantage gained from the use of the micro-technique.

The maximum intensity of each spot was estimated visually by comparison with a standard scale. For the preparation of this scale the ultra-fine collimating system of a low-angle camera* (slit width 8 μ) was used to photograph the direct beam, with exposure times varying from 3 to 90 sec. A set of streaks of width comparable with that of the spots on the micro-photographs was obtained. The fibre photograph was projected, as for the measurement of the positions of reflexions, and the scale was displaced by hand across the photograph in the projector. The standard streaks were placed as close as possible to the spot whose intensity was being measured in order to eliminate, as far as possible, the effect of varying intensity of the background.

We must now consider how the measured values of photographic maximum intensity are related to the R-space integrated intensities of reflexions. The relationship will depend on the following factors:

(i) *True diffraction breadth.*—The breadth of the reflexions, measured along a line joining the reflexion to the origin, is approximately constant over the whole photograph. It may therefore be assumed that the true diffraction breadth is everywhere small compared with the geometrical broadening (direct beam size) and can be neglected.

(ii) *Spread of reflexions in R-space due to disorientation of the crystallies.*—(*a*) If the crystallites are perfectly aligned with respect to the fibre axis but in random orientation about this axis, each reflexion will be spread over a circle of radius ξ/λ. Maximum intensities must therefore be multiplied by ξ/λ in order to relate them to integrated intensities. (This accounts for the factor $2\pi\xi' = 2\pi\xi/\lambda$ which occurs in equation (1) but not in equation (3)). (*b*) Imperfect alignment of the crystallites with respect to the fibre axis results in a small angular spread, φ, (Fig. 2) of each reflexion

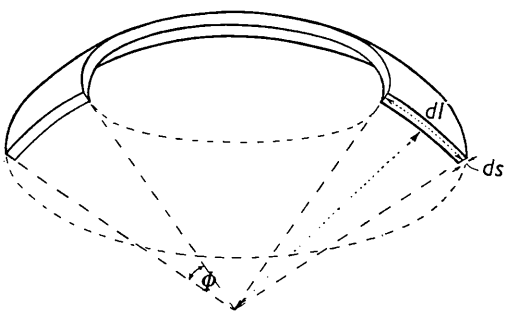

Fig. 2. Diagram illustrating spread of reflexion in reciprocal space.

along an arc of a circle with centre at the origin and the fibre axis as diameter. The length of this arc in R-space is equal to $s\varphi(=dl)$, where s is its distance from the origin. The R-space maximum intensity must therefore be multiplied by s to relate it to the integrated intensity.

(iii) *Geometrical factors involved in the transfer of R-space effects to the photographic film.*—We have seen that each reflexion will be spread, in R-space, over a small volume of circular symmetry with mean radius ξ/λ, and axis on the fibre axis. An axial section of this volume (Fig. 2) shows two elements each of area $ds.dl$, where ds is the true diffraction breadth of the reflexion and dl is the length of the arc resulting from disorientation of the crystallites with respect to the fibre axis. We must now consider the effect on the photographic maximum intensity of the oblique intersection of ds and dl with the reflecting sphere.

When a reflexion intersects the reflecting sphere obliquely two extreme effects are possible:

(*a*) If the diffraction breadth is much less than the geometrical breadth then the photographic spot size is independent of the diffraction breadth, and oblique intersection leads only to increased photographic

* Designed by K. P. Norris.

intensity. This is normally true in single-crystal work and is corrected for in the Lorentz factor.

(*b*) If the diffraction breadth is much greater than the geometrical breadth then oblique intersection with the reflecting sphere leads to increased spot breadth on the film but does not influence the maximum intensity.

In the present case we have seen that (*a*) is true for the dimension *ds*. Since *ds* makes an angle θ with the surface of the reflecting sphere, the observed maximum intensity must be multiplied by $\cos\theta$ to relate it to the integrated intensity.

In general, the effect of oblique intersection of *dl* with the reflecting sphere is important for all reflexions which occur at a large angular displacement from the equator. However, in the present work it happens that all such reflexions occur at diffraction angles large enough for the length of the photographic are to be much greater than the geometrical broadening (direct beam size). Oblique intersection of *dl* and the reflecting sphere is therefore without effect on the maximum intensity for these reflexions (see iii (*b*) above) and no special correction is required.

For reflexions at small diffraction angles and small angular displacement from the equator, the influence on the photographic maximum intensity of the geometrical broadening in the direction of *dl* is important. *dl* is given by $s\varphi$, where φ is the angular spread due to disorientation. To obtain φ a visual estimate was made of the half-peak length of the arcs for equatorial reflexions at large θ. (Since the value of the correction to be applied is in any case small, this method of estimation was considered adequate.)

This value of φ was then used to obtain the R-space lengths, *dl*, of arcs occurring at small θ. The lengths *dl'* of the photographic arcs for reflexions at small θ were then obtained from the *dl* values and the known diameter of the direct beam (by the method of Jones (1938)). If the effect of oblique intersection be neglected, the ratio of the R-space maximum intensity to the photographic maximum intensity is given by dl'/dl. The measured maximum intensity values must therefore be multiplied by this factor.

It is shown below that any error introduced by neglecting the obliquity correction for the reflexions at small θ has little effect on the resulting Patterson function.

We are now in a position to list all the corrections which must be applied to the observed maximum intensity values. They are:

1. Multiply by ξ/λ (see ii (*a*) above).
2. Multiply by $\cos\theta$ (see iii (*a*) above).
3. Multiply by s (see ii (*b*) above).
4. For reflexions at small θ, multiply by dl'/dl.
5. Multiply by the polarization factor $2/(1+\cos^2 2\theta)$.
6. Correct for the influence of the angle of incidence of the diffracted X-rays on the film (Cox & Shaw, 1930).
7. Correct for variation of specimen–film distance with θ for a flat film.
8. Correct for absorption.

Correction (8) was negligible throughout. Moreover, in the range of θ used in this study, corrections (2), (5), (6) and (7) taken together never exceed 10%, which is within the limit of experimental error of our intensity measurements. Only corrections (1), (3) and (4) were therefore used.

For the complete set of intensity measurements 12 films were used. These were obtained from two exposures on each of two different specimens, using three films for each exposure. The total range of intensities measured in this way was from 1 to 96, and agreement obtained between different sets of measurements was better than 20% for all except a few of the weakest reflexions. Some further error may have been introduced by the approximations involved in obtaining integrated from maximum intensities, but such error will vary only smoothly and slowly with s and will not, therefore, have a major influence on the main features of the Patterson diagram.

Artificial temperature factor

Since the corrected intensities showed little, if any, tendency to decrease with increasing θ an 'artificial temperature factor' was applied. Intensities were multiplied by $\exp[-a^2s^2]$ where $a = 4{\cdot}56$, a value chosen to reduce to 0·3 of its value the intensity of the furthest equatorial reflexion observed.

Calculation of the cylindrical Patterson function

Values of $J_0(u)$ were available only for values of u up to 40 (British Association, 1937; Clapp, 1937). In order to cover the desired range of $2\pi\xi' x$ in the present work, values of $J_0(u)$ for u up to 76 were required. These were calculated from the approximation formula $J_0(u) = (\sin u+\cos u)/\sqrt{(u\pi)}$. The results obtained are tabulated in the Appendix.

Values of the corrected intensities, $I(l, \xi')$, were then assembled for each layer line, l, and the summations of equation (3) were carried out at intervals of 1 Å in x in the range $x = 0$–50 Å. For each value of x, the required Patterson function is then given as a function of z by the cosine series of equation (2).

Results

The resulting cylindrically symmetrical Patterson function is shown in Fig. 3.

Before seeking in any way to interpret this function it seemed desirable to have some idea of the extent to which it might be influenced by possible errors in the intensity measurements. The greatest possible source of error lies in the two strongest spots, those at 11·3 Å on the equator and at 11·8 Å on the second layer line. Each of these is clearly an unresolved doublet, a fact which was allowed for only by making a visual

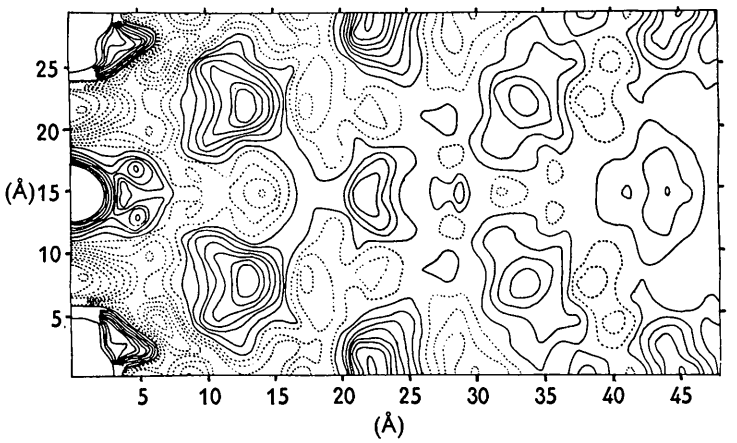

Fig. 3. Cylindrical Patterson function of NaDNA (structure *A*).

estimate of the breadth of the arc. Moreover, in the case of the second layer-line doublet, no correction was made for oblique intersection with the reflecting sphere (see above) and the intensity value adopted was therefore somewhat too high. It was estimated that, for these reflexions, the maximum possible error from all sources was about 30%. The Patterson function was therefore calculated for values of x up to 26 Å for these two doublets alone, and one-third of it was subtracted from the function shown in Fig. 3. The result is shown in Fig. 4. It is clear that the principal

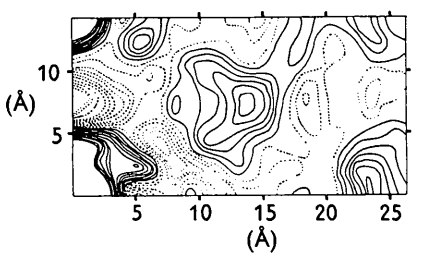

Fig. 4. Function shown in Fig. 3, with contribution of strong reflexions reduced by one third.

features of the function are substantially unaltered by this procedure, and that the effect of experimental error in intensity measurements is therefore not important.

The Patterson function shows a number of strong, well-defined peaks, and among these we must look for the lattice translations.

The first important region of high density occurs at x = 12–14 Å and z = 5–9 Å. However, it can readily be shown that it is impossible to index the equatorial reflexions on the basis of a unit cell in which one parameter has an x component of about 13 Å.

The peaks around x = 22 Å, z = 2 Å, and x = 40 Å, z = 0 were next selected as possibly containing lattice vectors. These agreed well with the $(b/a)\sin\beta$ ratio of 1·82 indicated by the application of a Bunn chart to the equatorial reflexions, and led to the satisfactory indexing of all the 66 observed reflexions on the basis of a *C*-face-centred monoclinic unit cell having the following parameters:

$$a = 22{\cdot}0,\ b = 39{\cdot}8,\ c = 28{\cdot}1\ \text{Å};\ \beta = 96{\cdot}5^\circ .$$

Agreement between calculated and observed values of ξ was generally better than 1%, and in no case worse than 2%.

It was found that for the larger values of θ on the equator and the first and second layer lines no reflexion could be indexed unambiguously; reflexions which should have been well-resolved and single were absent. This result is clearly not fortuitous. It seems to imply that the presence or absence of observable reflexions in this region is not of great significance; single reflexions are not strong enough to be distinguished from the rather strong diffuse background, and only where the geometry of the reciprocal lattice is such that two or more reflexions reinforce one another can a photographic effect be observed. On this account the introduction of an 'artificial temperature factor' mentioned above is more than usually important.

When all possible indices of the observed reflexions are taken into account the total number of reflexions is increased from 66 to 92.

Space group

Owing to the relatively small number of reflexions observed, and to the ambiguity of indexing the reflexions at large θ, systematic absences cannot be detected with certainty. However, since the asymmetric carbon atoms of the sugar rings preclude the existence of a plane of symmetry, *C*2 is the only space group possible.

Double orientation

A fortunate accident provided a rather satisfactory confirmation of the correctness of the indexing scheme. One fibre, of diameter about 40 μ, was found to give

a photograph showing strong double orientation; that is, the crystallites were not in random orientation about the fibre axis, and gave, as a result, something intermediate between a rotation and an oscillation photograph (Fig. 5). It will be seen that many pairs of equivalent reflexions in adjacent quadrants have markedly different intensities.

A list was drawn up in which those reflexions which were strongest in the top left-hand quadrant of this photograph were labelled L and those strongest in the top right-hand quadrant were labelled R. It was then found that all L reflexions had been allotted indices

Fig. 5. Single fibre, about 40 μ diameter. Specimen–film distance 15 mm.; r.h. 75%; exposure about 100 hr. Photograph showing double orientation.

hkl whereas all R reflexions had indices $hk\bar{l}$. The distribution of the observed reflexions among the different quadrants in R-space, as determined independently by the process of allotting indices, is thus directly confirmed by comparison with the distribution revealed in this photograph.

It was thought that the double orientation shown in Fig. 5 was probably due either to a mechanical accident to the fibre or to preferential orientation of the crystallites which lie near the surface. Two series of attempts to reproduce the effect in other fibres have, however, been unsuccessful. First, single fibres were placed on a glass slide and flattened by rolling a glass rod along the direction of the fibre axis. When air-dried fibres were used this resulted in a transformation to the unstable, optically positive state (Wilkins, Gosling & Seeds, 1951) which is highly disordered; that is, it had the same effect as excessive stretching. If, on the other hand, the fibres were rolled while at 75% r.h. they remained optically negative but showed subsequently the less highly ordered structure B (Franklin & Gosling, 1953*a*, Fig. 4). Secondly, X-ray photographs were taken of single fibres displaced with respect to the collimator in such a way that only a small region near the surface of the fibre was exposed to the X-rays. In this way several well-orientated photographs of structure A were obtained, but they showed no trace of double orientation.

Density determination

The density of NaDNA at various humidities was measured by the following method.

Homogeneous lumps of dry NaDNA were prepared by allowing pieces of swollen gel to dry slowly, stirring them gently at first to allow trapped air to escape. The lumps were then dried over P_2O_5 at room temperature for several weeks. To measure the density of the dry substance, each lump was placed in CCl_4 in a test tube, and the temperature was allowed to rise slowly from below $-10°$ C. until the lump just sank. In this way a density range of about 1·65–1·57 g.cm.$^{-3}$, corresponding to temperatures from $-10°$ C. to 30° C., can be satisfactorily covered. The density of dry NaDNA was found to be $1{\cdot}625\pm0{\cdot}002$ g.cm.$^{-3}$ at $4\pm1°$ C., in good agreement with Astbury's value of 1·63 g.cm.$^{-3}$ (Astbury, 1947).

By using, in the same temperature range, $CHCl_3$ in place of CCl_4 densities between about 1·54 and 1·47 g.cm.$^{-3}$ can be measured. Lumps of NaDNA were maintained at the required r.h. until equilibrium was reached and were then immersed in the appropriate liquid (CCl_4 or $CHCl_3$), the temperature of which was rapidly adjusted to give a density measurement. In this way the density of NaDNA at 75% r.h. was found to be $1{\cdot}471\pm0{\cdot}002$ g.cm.$^{-3}$ (corresponding to a temperature of $30\pm1°$ C. in $CHCl_3$). The water uptake of the lumps at 75% r.h. was 34–38%.

Number of nucleotides per unit cell

We are now in a position to assign upper and lower limits to the number of nucleotides per unit cell. The value cannot be fixed precisely owing to the uncertainty in the quantity of water in the crystallites (Franklin & Gosling, 1953*a*); this in turn leads to some uncertainty in the density of the crystallites, which may well be slightly greater than the value measured for the bulk material at 75% r.h.

In Table 2 we show the number of nucleotides per face-centred unit cell, calculated for water contents

Table 2. *Number of nucleotides per unit cell*

Mean molecular weight of dry nucleotide = 330
Density of NaDNA at r.h. 75% = 1·471 g.cm.$^{-3}$

No. of molecules of water per nucleotide	Molecular weight; nucleotide and water	Water content %	No. of nucleotides per unit cell
4	402	21·8	54·0
5	420	27·3	51·6
6	438	33·0	49·5
7	456	38·2	47·5
8	474	43·6	45·7

of the crystallites corresponding to from 4 to 8 molecules of water per nucleotide, and assuming a density of 1·47 g.cm.$^{-3}$ for the crystallites.

Table 3. *Zero-order Bessel function*

u	$J_0(u)$	u	$J_0(u)$	u	$J_0(u)$	u	$J_0(u)$
40·058	0	49·4	−0·0091	58·4	0·0502	67·4	−0·0778
40·4	−0·0421	49·7	0·0244	58·7	0·0210	67·7	−0·0569
40·7	−0·0752	50·0	0·0561	59·0	−0·0108	68·0	−0·0311
41·0	−0·1010	50·3	0·0825	59·3	−0·0401	68·3	−0·0026
41·3	−0·1176	50·6	0·1011	59·6	−0·0664	68·6	0·0260
41·6	−0·1236	50·9	0·1106	59·9	−0·0866	68·9	0·0521
41·9	−0·1185	51·2	0·1102	60·2	−0·0997	69·2	0·0734
42·2	−0·1032	51·5	0·1001	60·5	−0·1025	69·5	0·0882
42·5	−0·0786	51·8	0·0809	60·8	−0·0968	69·8	0·0951
42·8	−0·0471	52·1	0·0549	61·1	−0·0826	70·1	0·0934
43·1	−0·0118	52·4	0·0237	61·4	−0·0611	70·4	0·0834
43·4	0·0244	52·7	−0·0088	61·7	−0·0343	70·7	0·0660
43·7	0·0582	53·0	−0·0407	62·0	−0·0045	71·0	0·0428
44·0	0·0866	53·3	−0·0688	62·3	0·0256	71·3	0·0159
44·3	0·1070	53·6	−0·0906	62·2	0·0532	71·6	−0·0123
44·6	0·1177	53·9	−0·1040	62·9	0·0760	71·9	−0·0393
44·9	0·1180	54·2	−0·1084	63·2	0·0917	72·2	−0·0626
45·2	0·1076	54·5	−0·1030	63·5	0·0994	72·5	−0·0804
45·5	0·0879	54·8	−0·0884	63·8	0·0982	72·8	−0·0907
45·8	0·0604	55·1	−0·0660	64·1	0·0882	73·1	−0·0932
46·1	0·0278	55·4	−0·0379	64·4	0·0704	73·4	−0·0871
46·4	−0·0072	55·7	−0·0065	64·7	0·0463	73·7	−0·0734
46·7	−0·0413	56·0	0·0252	65·0	0·0183	74·0	−0·0532
47·0	−0·0715	56·3	0·0546	65·3	−0·0112	74·3	−0·0369
47·3	−0·0952	56·6	0·0797	65·6	−0·0396	74·6	−0·0075
47·6	−0·1102	56·9	0·0960	65·9	−0·0644	74·9	0·0263
47·9	−0·1152	57·2	0·1046	66·2	−0·0832	75·2	0·0511
48·2	−0·1101	57·5	0·1036	66·5	−0·0946	75·5	0·0713
48·5	−0·0950	57·8	0·0937	66·8	−0·0975	75·8	0·0851
48·8	−0·0720	58·1	0·0753	67·1	−0·0917	76·1	0·0912
49·1	−0·0423						

Discussion

It has been shown that the use of the cylindrically symmetrical Patterson function has enabled the unit cell to be established for the most highly ordered state of the sodium desoxyribonucleate obtained from calf thymus. For subsequent stages in the elucidation of this structure, methods used in the determination of the structure of single crystals can therefore be applied. Work on the three-dimensional Patterson function is now in progress and will be described in a later paper. Since this is a much more powerful instrument than the cylindrical function, no attempt will be made to introduce hypotheses concerning details of structure at the present stage. A few comments of a general nature may, however, be made.

The Patterson function shows rather few peaks of remarkably high intensity relative to that of the peak at the origin. Since the unit cell contains a very large number of atoms (of the order of 1000, excluding hydrogen and water) it seems probable that the main features of the function represent phosphate–phosphate interactions, these being the heaviest group in the structure.

It will be observed that the *C*-face-centred monoclinic unit cell is near-hexagonal in projection. Nevertheless, there is evidence to suggest that the symmetry of the crystallite itself is far from cylindrical. Although the nature of the accident which produced double orientation of the crystallites in a fibre (Fig. 5) is unknown, it seems unlikely that it could have occurred at all if the individual crystallites had a high degree of symmetry about the fibre axis.

Note added in proof, 8 *July* 1953.—Since this paper was written, Watson & Crick (1953) have proposed a two-chain helical structure for nucleic acid. Their model might be expected to relate to our structure *B*, in which the molecules are protected by a sheath of water from the distorting influence of neighbouring molecules, rather than to structure *A*. Nevertheless, since the change $A \rightleftharpoons B$ is readily reversible, if a two-chain helical molecule exists in structure *B* it must persist as such in structure *A*, though the dimensions of the helix may be altered. We have shown (Franklin & Gosling, 1953*b*, *c*) that the general features of the model proposed by Watson & Crick appear to be consistent with our results, though discrepancies between observed and calculated equatorial intensities in structure *B*, and between observed and calculated density values, prevent us from accepting it in detail.

APPENDIX

Zero-order Bessel function $J_0(u)$

The function $J_0(u)$ calculated for $u = 40$–76 from the approximation formula $J_0(u) = (\sin u + \cos u)/\sqrt{(\pi u)}$ at intervals of $u = 0{\cdot}3$ and to accuracy of $\pm 0{\cdot}0002$ in $J_0(u)$ is given in Table 3.

References

ASTBURY, W. T. (1947). *Cold Spring Harbour Symposium on Quantitative Biology*, **12**, 56.

BRITISH ASSOCIATION FOR THE ADVANCEMENT OF SCIENCE (1937). *Mathematical Tables*, Vol. 6, Part 1. Cambridge: University Press.

CLAPP, M. M. (1937). *J. Math. Phys.* **16**, 76.

COX, E. G. & SHAW, W. F. B. (1930). *Proc. Roy. Soc.* A, **127**, 71.

FRANKLIN, R. E. & GOSLING, R. G. (1953*a*). *Acta Cryst.* **6**, 673.

FRANKLIN, R. E. & GOSLING, R. G. (1953*b*). *Nature, Lond.* **171**, 742.

FRANKLIN, R. E. & GOSLING, R. G. (1953*c*). *Nature, Lond.* **172**, 156.

JONES, F. W. (1938). *Proc. Roy. Soc.* A, **166**, 16.

MACGILLAVRY, C. H. & BRUINS, E. M. (1948). *Acta Cryst.* **1**, 156.

WATSON, J. D. & CRICK, F. H. C. (1953). *Nature, Lond.* **171**, 737.

WILKINS, M. H. F., GOSLING, R. G. & SEEDS, W. E. (1951). *Nature, Lond.* **167**, 759.

Acta Cryst. (1953). **6**, 685

The Fourier Transform of a Coiled-Coil

BY F. H. C. CRICK

The Medical Research Council Unit for the Study of the Molecular Structure of Biological Systems, The Cavendish Laboratory, Cambridge, England

(*Received* 14 *March* 1953)

The Fourier transforms are given for a continuous coiled-coil, and for a set of atoms spaced at regular intervals along a coiled-coil. The nature of the solution is briefly discussed.

Introduction

It has recently been suggested simultaneously by Pauling & Corey (1953) and by Crick (1952) that the structure of α-keratin may be based on a coiled-coil, i.e. on a helix with a small repeat whose axis has been slightly deformed so that it follows a larger more gradual helix. The small helix proposed is the α-helix of Pauling, Corey & Branson (1951).

It is therefore of interest to calculate the Fourier transform (or continuous structure factor) of structures of this sort. Those considered here are the continuous coiled-coil and the discontinuous coiled-coil. The former is an infinitely thin 'wire' of electron density, and the latter is a set of scattering points (atoms) placed at regular intervals on a coiled-coil locus. It will be shown that the two results are very closely related.

To obtain the structure factors for a structure of this type made up of real atoms, one follows a similar procedure to that described by Cochran, Crick & Vand (1952) in calculating the transform of the simple α-helix, i.e. one considers the atoms as being in sets, each set consisting of one atom from each residue. Thus all the nitrogen atoms of the polypeptide backbone will be in one set, all the oxygen atoms of the backbone in another, and so on. One then uses the formula derived in this paper to calculate the contribution of each set separately, allowance being made for the finite size of the atom by multiplying the result for a set of points by the appropriate atomic scattering factor in the usual way. The results are then added together, with proper allowance for phase, to give the structure factor for the complete structure.

The advantage of a general solution of the type given here is that instead of calculating the contribution of each atom separately one can group them into sets, in this case with a large number in each, and calculate the whole contribution of a set at one go.

We shall call the small helix the minor helix and the larger helix followed by its axis the major helix.

Mathematical method

A general description is given first, and the particular case of the coiled-coil is then derived afterwards.

Consider first the problem of a continuous infinitely thin 'wire' of electron density. Let us suppose that it is defined parametrically in terms of a parameter, t, which may be proportional to the length along the wire, though this is not essential. We also assume that the structure repeats exactly after a distance c in the z direction.

We can form the expression for the value of the Fourier transform of such a wire at some particular point in reciprocal space. We will call this $C(R, \psi, Z)$, where R, ψ and Z are the cylindrical co-ordinates of the point in reciprocal space under consideration.

Now it will often happen that the expression for the transform at this point will be an integral of the form

$$C(R, \psi, Z) = \int_0^{t_0} f_1(t) f_2(t) f_3(t)\, dt\,,$$

where t_0 is the value of t after which the structure repeats, and $f_1(t)$, $f_2(t)$ and $f_3(t)$ are simple functions of t. They may also be functions of R, ψ and Z, but for the moment we are considering these as fixed.